AUT Journal of Mechanical Engineering

AUT J. Mech. Eng., 6(1) (2022) 129-148
DOI: 10.22060/ajme.2021.19819.5967

Two-Phase Simulation of Magnetohydrodynamics and Ferrohydrodynamics Impacts on the Natural Convection of a Magnetic Nanofluid within a Porous Cavity

S. Goudarzi , S. Yekani Motlagh, H. Soltanipour*

Department of Mechanical Engineering, Urmia University of Technology, Urmia, Iran

ABSTRACT: This article attempts to evaluate the impact of magnetohydrodynamics and ferrohydrodynamics on the free convection of a magnetic nanofluid in a square porous cavity. The published literature shows that the magnetic nanofluid convection problems have been mostly simulated by the single-phase model. In the present work, a two-phase model is used to consider the effects of Brownian diffusion, thermophoresis, and magnetophoresis of particles. The Darcy-Brinkman formulation is employed to treat mass, momentum, and energy transport phenomena in the porous medium. The governing equations are solved numerically by the finite volume technique. Numerical computations are performed for various Rayleigh numbers ($Ra=10^4$ and $Ra=10^5$), Hartmann numbers ($0\le Ha\le 5$), magnetic numbers ($0\le Mn\le 4\times10^7$), and porosity ratio of $\varepsilon=0.5$ and 0.9. The current results are validated via comparison with existing experimental or numerical results in the literature. Impacts of magnetohydrodynamics, ferrohydrodynamics, and ferrohydrodynamics/magnetohydrodynamics on the flow field and heat transfer rate are discussed separately in detail by contour plots of streamlines, isotherms, and distribution profiles of nanoparticles. Numerical results indicate that at $Ra=10^4$ heat is mainly transferred by conduction and its rate is unaffected by porosity, magnetic, or Hartmann numbers. However, at $Ra=10^6$ and $\varepsilon=0.9$ the average Nusselt number decreases by increasing magnetic and Hartmann numbers.

Review History:

Received: Apr. 04, 2021
Revised: Jul. 22, 2021
Accepted: Aug. 25, 2021
Available Online: Sep. 01, 2021

Keywords:

Ferrohydrodynamics
Magnetic nanofluid
Magnetohydrodynamics
Porous medium
Two-phase modeling

1- Introduction

Because of numerous applications in nature, engineering, and industry (including electronic cooling, solar collectors, crystal growth, thermal storage systems, etc.), the analysis of natural convection in cavities has fascinated many investigators. In the last two decades, nanofluids have been one of the most effective fluids for heat transfer purposes. The experimental measurements of Choi and Eastman [1] revealed that the heat transfer performance of common liquids can be considerably improved by dispersing metallic nanoparticles.

One of the first numerical studies on the nanofluids was performed by Khanafer et al.[2]. They reported the free convection of nanofluids in an enclosure. Their numerical analysis confirmed that the rate of heat transfer is increased via nanofluids. The majority of the existing numerical investigations concerning the heat transfer of nanofluids are carried out by the single-phase approach that is all possible relative motions of nanoparticles in the base fluid are neglected. For example, nanofluid natural convection in a semi-annulus cavity was numerically investigated by Soleimani et al. [3]. They found that at any Rayleigh number, there is an angle of turn with a maximum heat exchange rate. Sheikholeslami et al. [4] investigated the free convection of a nanofluid in a cavity composed of an inner elliptic cylinder and an outer circular one. It was demonstrated that the rate of convection increases with enhancing nanoparticle void fraction, Rayleigh number, and inclination angle of the elliptic cylinder. Soltanipour et al. [5] reported the efficacy of a variable magnetic field on the nanofluid convection heat transfer in a 2D channel. They stated that an applied magnetic field considerably enhances the heat transfer rate. Some studies corroborated that the two-phase treatment of nanofluids is more accurate results than the single-phase approach [6, 7]. The mixture model has been mostly used in the simulation of nanofluids [8-11]. Buongiorno [12] introduced a new two-phase model that has received significant attention in recent years. By comparing different slip mechanisms, the author concluded that the Brownian and thermophoresis diffusions play a dominant role in the dispersion of nanoparticles. Corcione et al. [13] declared that Buongiorno's two-phase model accuracy is higher than the single-phase method in simulating the free convection of nanofluids. Some investigators employed Buongiorno's two-phase model to study nanofluid natural convection [14-16].

Compared to other nanofluids, magnetic nanofluids have a prominent property of magnetization. This unique feature has made them widely used in medicine and engineering [17-20]. Utilizing the Lattice Boltzmann Method (LBM), Kefayati [21] analyzed the role of an external field in the

*Corresponding author's email: h.soltanipour@gmail.com

natural convection of a magnetic nanofluid within a cavity. Results showed that an externally- applied magnetic field is more effective at high Rayleigh numbers. Sheikholeslami and Gorji [22] studied the natural convection of a magnetic fluid in a bottom heated square cavity under a magnetic field. It was concluded that the rate of heat transport increases with increasing the Rayleigh number and length of heat source. Tzirtzilakis and Xenos [23] studied the effects of Ferrohydrodynamic and Magnetohydrodynamic on biomagnetic fluid flow in a lid-driven cavity. It was found that the flow pattern is strongly affected by the Hartmann and magnetic numbers. Recently, nanofluid natural convection inside saturated porous media has received much attention. A literature survey shows that the two-phase modeling of nanofluids in porous media is relatively rare, and most of them were performed using the single-phase method [24]. Sheremet et al. [25, 26] reported the results of Buongiorno's two-phase model for the prediction of natural convection of nanofluids inside 2D and 3D porous enclosures. A two-phase simulation of nanofluid free convection in a tilted porous enclosure was done by Motlagh et al. [27]. Their numerical results indicated that at large porous Rayleigh numbers, the porosity ratio strongly affects the rate of heat transport. Motlagh et al. [28] implemented a two-phase simulation of nanofluid natural convection in a half-annulus porous cavity. An examination of the effect of the tilt angle of the cavity, porous Rayleigh number, porosity, and void fraction of nanoparticles, revealed that the rate of heat transfer increases with increasing the porosity ratio.

The present paper seeks to elucidate the Ferrohydrodynamics (FHD) and Magnetohydrodynamics (MHD) effects on a magnetic nanofluid natural convection in a porous medium. For this purpose, the two-phase model of Buongiorno has been extended to consider the magnetophoresis effects. To the best knowledge of the authors, such an investigation has not been reported before. The impact of some effective parameters such as magnetic, Hartmann, and Rayleigh numbers, as well as the porosity ratio of the porous medium on the flow variables, are presented in the following sections.

2- Mathematical Modeling

2- 1- Problem statement

The objective of the current work is to determine the Ferrohydrodynamics (FHD) and Magnetohydrodynamics (MHD) influences on the convective heat transport of water/Fe_3O_4 magnetic nanofluid in a saturated porous medium. The schematic presentation of the problem is shown in Fig. 1.

As shown in Fig. 1, the left and right vertical walls have constant temperatures, T_h and T_c while the horizontal walls are insulated. The origin of the coordinate system is at the left bottom corner of the enclosure. Magnetic nanofluid is subjected to non-uniform magnetic fields of eight current-carrying wires, which provide FHD effects. The location of each magnetic source is depicted in the figure. For wires w1-w4, an electrical current flows in the positive z-direction while for the remaining wires current is in the opposite direction. Moreover, a uniform magnetic field of ($\vec{\mathbf{B}} = B_z \hat{\mathbf{k}}$) is applied to the ferrofluid in the positive z-direction. Such a magnetic field provides MHD effects.

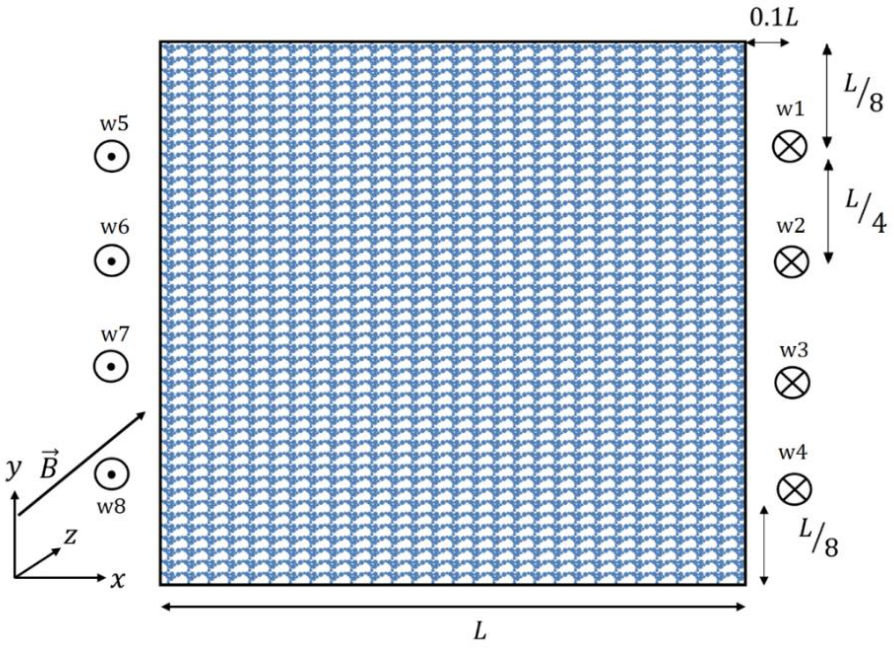

Fig. 1. Geometry of the problem

2- 2- Governing equations and boundary conditions

Magnetic nanofluid flow is taken to be 2D, laminar, incompressible, steady-state, and Newtonian. The Darcy-Brinkman model is used for the formulation of ferrofluid flow in a porous medium which is considered as a homogeneous and isotropic material. Moreover, ferrofluid and solid matrix are considered to be in the Local Thermal Equilibrium (LTE). The Boussinesq law is utilized to approximate the density variation of ferrofluid in the buoyancy term. It is assumed that the applied magnetic fields have negligible effects on the thermophysical properties of magnetic nanofluid. Also, the magnetocaloric effect, thermal radiation, and viscous dissipation are neglected. In this study, the Buongiorno two-phase model is extended to incorporate the magnetophoresis diffusion of nanoparticles in the base fluid. Based on these assumptions, the governing equations for continuity, momentum, energy, and nanoparticle void fraction are as follows [12, 23, 29]:

$$\nabla.\vec{\mathbf{V}} = 0 \tag{1}$$

$$\begin{aligned}&\frac{1}{\varepsilon^2}(\rho_{nf}\,\vec{\mathbf{V}}.\nabla\vec{\mathbf{V}}) = -\nabla\vec{\mathbf{V}} - \frac{\mu_{nf}}{K}\vec{\mathbf{V}} + \\ &\nabla.(\frac{\mu_{nf}}{\varepsilon}\nabla\vec{\mathbf{V}}) + (\rho\beta)_{nf}(T - T_c)\mathbf{e_g} + \\ &\mu_0(\mathbf{M}.\nabla)\vec{\mathbf{H}} - \sigma_{nf}(\vec{\mathbf{V}}\times\vec{\mathbf{B}}\times\vec{\mathbf{B}})\end{aligned} \tag{2}$$

$$(\rho c)_{nf}\,\vec{\mathbf{V}}.\nabla T = \nabla.(k_{nf,eq}\nabla T) - \varepsilon c_p\,\overrightarrow{\mathbf{J_p}}.\nabla T \tag{3}$$

$$\frac{1}{\varepsilon}\vec{\mathbf{V}}.\nabla\varphi = -\frac{1}{\rho_p}\nabla.(\overrightarrow{\mathbf{J_p}}) \tag{4}$$

where $\vec{\mathbf{V}} = (u, v)$ is velocity field; P and T are pressure and temperature; $\mathbf{e_g}$ is the unit vector in the negative y-direction; ε is porosity and K refers to permeability; σ_{nf} denotes the electrical conductivity of nanofluid. Also μ_0 is the permeability of vacuum; $\vec{\mathbf{H}}$, $\vec{\mathbf{B}}$ and $\mathbf{M}$ are the magnetic field intensity, flux density, and magnetization vectors, respectively and $\vec{\mathbf{B}} = \mu_0\vec{\mathbf{H}}$. Also, subscript "nf" and "p" denote nanofluid and nanoparticles. The terms $\mu_0(\mathbf{M}.\nabla)\vec{\mathbf{H}}$ and $-\sigma_{nf}(\vec{\mathbf{V}}\times\vec{\mathbf{B}}\times\vec{\mathbf{B}})$ on the right side of momentum equations are the Kelvin and Lorentz body forces, respectively. The components of the magnetic field and its magnitude are as follows [23]:

$$\begin{cases} H_x = \sum_{i=1}^{4}\dfrac{I}{2\pi}\dfrac{(y-y_i)}{(x-x_i)^2+(y-y_i)^2} \\ H_y = \sum_{i=1}^{4}\dfrac{-I}{2\pi}\dfrac{(x-x_i)}{(x-x_i)^2+(y-y_i)^2} \end{cases} \tag{5}$$

$$\begin{cases} H_x = \sum_{i=5}^{8}\dfrac{-I}{2\pi}\dfrac{(y-y_i)}{(x-x_i)^2+(y-y_i)^2} \\ H_y = \sum_{i=5}^{8}\dfrac{I}{2\pi}\dfrac{(x-x_i)}{(x-x_i)^2+(y-y_i)^2} \end{cases} \tag{6}$$

$$H_z = B_z \big/ \mu_0 \tag{7}$$

$$H = [(\sum H_x)^2 + (\sum H_y)^2 + {H_z}^2]^{1/2} \tag{8}$$

where (x_i, y_i) denotes the coordinates of i-th magnetic source, and I is the current intensity.

Langevin law is used to compute the magnetization of ferrofluid [30]:

$$M = M_s L(\xi) \tag{9}$$

where M_s is the saturation magnetization of ferrofluid and $L(\xi)$ refers to Langevin function which is defined as:

$$L(\xi) = \coth(\xi) - \frac{1}{\xi} \tag{10}$$

In the above equation, $\xi = \dfrac{\mu_0 m_p H}{k_B T}$ is the Langevin parameter and $m_p = \dfrac{4\mu_B \pi {d_p}^3}{6\times 91.25\times 10^{-30}}$ refers to the magnetic moment of nanoparticles [30]. Moreover, φ and m_p stand for particle volume fraction and particle's diameter respectively, $k_B = 1.380648\times 10^{-23}$ J/K is the Boltzmann constant and $\mu_B = 9.724\times 10^{-24}$ J/T is the Bohr magneton.

In Eq. (3), $\mathbf{J_p}$ is the nanoparticle's mass flux, which can be written as:

$$\overrightarrow{\mathbf{J_P}} = \overrightarrow{\mathbf{J_B}} + \overrightarrow{\mathbf{J_T}} + \overrightarrow{\mathbf{J_M}} \tag{11}$$

where $\overrightarrow{\mathbf{J_B}}$ and $\overrightarrow{\mathbf{J_T}}$ are the mass fluxes because of Brownian and thermophoresis effects, and $\overrightarrow{\mathbf{J_M}}$ denotes the magnetophoretic flux. $\overrightarrow{\mathbf{J_B}}$, $\overrightarrow{\mathbf{J_T}}$ and $\overrightarrow{\mathbf{J_M}}$ d are computed from [31]:

$$\overrightarrow{\mathbf{J_B}} = -\rho_p D_B \nabla\varphi \tag{12}$$

$$\overrightarrow{\mathbf{J_T}} = -\rho_p D_T \frac{\nabla T}{T} \tag{13}$$

$$\overrightarrow{\mathbf{J_M}} = \rho_p D_B (\frac{\varphi}{H}) \xi L(\xi) \nabla H \tag{14}$$

The Brownian diffusion is calculated from [12]:

$$D_B = \frac{k_B T}{3\pi \mu_f d_p} \tag{15}$$

The thermophoresis coefficient D_T is determined by the following equation:

$$D_T = \gamma \frac{\mu_f}{\rho_p} \varphi \tag{16}$$

where γ is a constant and defined as $\gamma = \frac{0.26 k_f}{2k_f + k_p}$ [12].

Substituting of Eqs. (11) to (14) into nanoparticle's void fraction equation yields:

$$\frac{1}{\varepsilon} \vec{\mathbf{V}} . \nabla \varphi = \nabla . [D_B \nabla \varphi + D_T \frac{\nabla T}{T} - D_B (\frac{\varphi}{H}) \xi L(\xi) \nabla H] \tag{17}$$

The following boundary conditions are applied:

on the horizontal walls $\nabla T . \mathbf{n} = 0$

$$\vec{\mathbf{V}} = 0 \qquad \nabla \varphi . \mathbf{n} = \left(\frac{\varphi}{H} \right) \xi L(\xi) \nabla H . \mathbf{n} \tag{18}$$

on the left wall $T = T_h$

$$\vec{\mathbf{V}} = 0 \qquad \nabla \varphi . \mathbf{n} = -\frac{D_T}{D_B} \nabla T . \mathbf{n} + (\frac{\varphi}{H}) \xi L(\xi) \nabla H . \mathbf{n} \tag{18}$$

on the right wall $T = T_c$

$$\vec{\mathbf{V}} = 0 \qquad \nabla \varphi . \mathbf{n} = -\frac{D_T}{D_B} \nabla T . \mathbf{n} + (\frac{\varphi}{H}) \xi L(\xi) \nabla H . \mathbf{n} \tag{18}$$

In the above equations, $\mathbf{n}$ is a unit vector normal to a boundary.

2- 3- Thermophysical properties of magnetic nanofluid

The following relations are used to determine the density, specific heat, and volume expansion coefficient of magnetic nanofluid [32, 33]:

$$\rho_{nf} = (1-\varphi)\rho_f + \varphi \rho_p \tag{19}$$

$$(\rho c)_{nf} = (1-\varphi)(\rho c)_f + \varphi (\rho c)_p \tag{20}$$

$$(\rho \beta)_{nf} = (1-\varphi)(\rho \beta)_f + \varphi (\rho \beta)_p \tag{21}$$

The viscosity of nanofluid is calculated based on the Brinkman equation [34]:

$$\mu_{nf} = \frac{\mu_f}{(1-\varphi)^{2.5}} \tag{22}$$

Ferrofluid thermal conductivity is estimated by the Hamilton-crosser model [35]:

$$k_{nf} = \frac{k_p + 2k_f - 2\varphi(k_p - k_f)}{k_p + 2k_f + \varphi(k_p - k_f)} \tag{23}$$

Maxwell model is used to approximate the electrical conductivity of the mixture [36]:

$$\sigma_{nf} = \sigma_f [1 + \frac{3(\frac{\sigma_p}{\sigma_f} - 1)\varphi}{(\frac{\sigma_p}{\sigma_f} + 2) - (\frac{\sigma_p}{\sigma_f} - 1)\varphi}] \tag{24}$$

The effective conductivity in porous media can be calculated as below [37]:

$$k_{nf,eq} = \varepsilon k_{nf} + (1-\varepsilon) k_s \tag{25}$$

The thermophysical properties used in this study are listed in Table 1.

Table 1. Thermophysical properties of water, Fe_3O_4 nanoparticles, and solid matrix [16, 27, 38]

Physical properties	water	Fe_3O_4	porous medium
c (J/kg.K)	4178	670	-
σ (1/Ω.m)	0.05	25000	-
ρ (kg/m^3)	993	5200	-
β×10^5 (1/K)	36.2	1.3	-
μ×10^6 (Pa.s)	695	-	-
k (W/m.K)	0.628	6	100

2- 4- Non-dimensionalisation of the governing equations

The nondimensionalized form of the governing equations can be obtained by the following parameters [12, 16, 39]:

$$(x^*, y^*) = (\frac{x}{L}, \frac{y}{L}), \nabla^* = L\nabla, T^* = \frac{T - T_C}{T_h - T_C},$$

$$V^* = \frac{VL}{\nu_f}, P^* = \frac{PL^2}{\rho_f {\nu_f}^2}, H^* = \frac{H}{H_0}, H_0 = \frac{I}{2\pi\lambda},$$

$$B^* = \frac{B}{B_0}, M^* = \frac{M}{M_0}, M_0 = M(\varphi_{ave}, T_C),$$

$$\varphi^* = \frac{\varphi}{\varphi_{ave}}, \delta = \frac{T_C}{T_h - T_C}, D_B{}^* = \frac{D_B}{D_{B0}},$$

$$D_T{}^* = \frac{D_T}{D_{T0}}, D_{T0} = \gamma \frac{\mu_f}{\rho_f}\varphi_{ave}, D_{B0} = \frac{k_B T_C}{3\pi\mu_f d_p},$$

$$Mn = \frac{\mu_0 H_0 M_0 L^2}{\rho_f {\nu_f}^2}, \Pr = \frac{\nu_f}{\alpha_f}, Da = \frac{K}{L^2},$$

$$Ha = B_Z L\sqrt{\frac{\sigma_f}{\mu_f}}, Ra_f = \frac{g\beta_f (T_h - T_C)L^3}{\alpha_f \nu_f},$$

$$Le = \frac{k_f}{(\rho c_p) D_B \varphi_{ave}}, N_{BT} = \frac{\varphi_{ave} D_{B0} \delta}{D_{T0}},$$

Therefore, the non-dimensional representation of governing equations are as follows:

$$\nabla^* V^* = 0 \tag{26}$$

$$\begin{aligned}&\frac{1}{\varepsilon^2}(\frac{\rho_{nf}}{\rho_f})\mathbf{V}^*\nabla^*.\mathbf{V}^* = -\nabla^* P^* - \\ &(\frac{\mu_{nf}}{\mu_f})\frac{1}{Da}V^* + \frac{1}{\varepsilon}\nabla^*.(\frac{\mu_{nf}}{\mu_f}\nabla^* V^*) + \\ &\frac{(\rho\beta)_{nf}}{(\rho\beta)_f}\frac{1}{Pr}RaT^*\mathbf{e_g} + \\ &Mn(\mathbf{M}^*.\nabla)\mathbf{H}^* + (\frac{\sigma_{nf}}{\sigma_f})Ha^2\mathbf{V}^*\end{aligned} \tag{27}$$

$$\begin{aligned}&\frac{(\rho c)_{nf}}{(\rho c)_f}V^*.\nabla^* T^* = \frac{1}{\Pr}\nabla^*.\left(\left(\frac{k_{nf,eff}}{k_f}\right)\nabla^* T^*\right) - \\ &\varepsilon\frac{1}{\Pr}\frac{1}{Le}[D_B{}^*\nabla^*\varphi^*.\nabla^* T^* + \\ &\frac{1}{N_{BT}}D_T{}^*\frac{\nabla^* T^*.\nabla^* T^*}{1+\delta T^*} - \\ &D_B{}^*\xi L(\xi)\varphi^*\frac{\nabla^* H^*.\nabla^* T^*}{H^*}]\end{aligned} \tag{28}$$

$$\begin{aligned}&\frac{1}{\varepsilon}V^*.\nabla^*\varphi^* = \frac{1}{Sc}\nabla^*.(D_B{}^*\nabla^*\varphi^* + \\ &\frac{1}{N_{BT}}D_T{}^*\frac{\nabla^* T^*}{1+\delta T^*} - D_B{}^*\xi L(\xi)\varphi^*\frac{\nabla^* H^*}{H^*})\end{aligned} \tag{29}$$

The boundary conditions in the dimensionless forms are as follows:

on the horizontal walls $\nabla T^{*}.n=0$

$$V^{*}=0 \quad \nabla^{*}\varphi^{*}.n=\left(\frac{\varphi^{*}}{H^{*}}\right)\xi L(\xi)\nabla H^{*}.n \tag{30}$$

on the left wall $T^{*}=1$

$$V^{*}=0 \quad \nabla^{*}\varphi^{*}.n=-\frac{1}{N_{BT}}\frac{D_T^{*}}{D_B^{*}}\frac{\nabla^{*}T^{*}.n}{1+\delta T^{*}}+\xi L(\xi)\varphi^{*}\frac{\nabla^{*}H^{*}.n}{H^{*}} \tag{30}$$

on the right wall $T^{*}=0$

$$V^{*}=0 \quad \nabla^{*}\varphi^{*}.n=-\frac{1}{N_{BT}}\frac{D_T^{*}}{D_B^{*}}\frac{\nabla^{*}T^{*}.n}{1+\delta T^{*}}+\xi L(\xi)\varphi^{*}\frac{\nabla^{*}H^{*}.n}{H^{*}} \tag{30}$$

The average Nusselt number is obtained by integrating the local Nusselt number along the hot vertical wall of the cavity:

$$Nu_m=\frac{1}{2}\left[\left(\int_0^1\frac{k_{nf,eq}}{k_f}\frac{\partial T^{*}}{\partial x^{*}}\right)_{X^{*}=0}dy^{*}+\left(\int_0^1\frac{k_{nf,eq}}{k_f}\frac{\partial T^{*}}{\partial x^{*}}\right)_{X^{*}=1}dy^{*}\right] \tag{31}$$

3- Numerical Procedure

The governing equations of the problem are solved by the well-known finite volume technique and on a co-located mesh [40]. It should be mentioned that the constitutive relations for thermophysical properties of nanofluid, Brownian, and thermophoresis diffusion coefficients and magnetization of the ferrofluid are updated at each iteration since they vary with void fraction and temperature. In this study, a central difference scheme is employed to discretize the diffusive fluxes while the convective ones are treated by an upwind method. Also, the Semi-Implicit Method for Pressure Linked Equations (SIMPLE) method is utilized for coupling velocity and pressure fields. The numerical solution starts with the single-phase method and after some iterations is switched to two phase-model. To obtain the converged solution, the proper values of under relaxation factors are used. The termination criterion is satisfied as soon as all residuals become less than 10^{-6}.

3- 1- Grid independent study

To ensure that the obtained results are grid-independent, various uniform grids are tested. Table 2 presents the grid study validation test for the case of $Ra=10^{6}$, $Ha=1$, $\varepsilon=0.9$, and $Mn=4\times10^{7}$ As seen, for the mesh size of 200×200, the solution becomes grid-independent.

3- 2- Validation

Verification is done by the comparison of present results with other published ones. The present results first are compared with the experimental results of Ho et al. [41] and the numerical results of Sheikhzadeh et al. [42] for free convection of Al_2o_3/water nanofluid in a differentially heated enclosure. This comparison is illustrated in Fig. 2. The average

Table 2. Grid study at $Ra=10^{6}$, $Ha=1$, $\varepsilon=0.9$ $Mn=4\times10^{7}$ and

$n_x\times n_y$	150×150	180×180	200×200	230×230	250×250
Nu_m	1.676	1.661	1.659	1.657	1.656

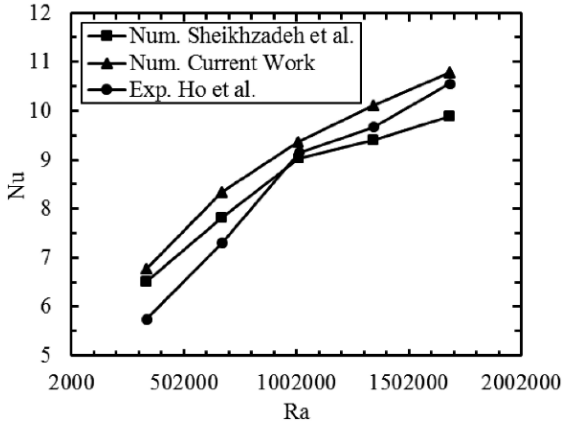

Fig. 2. Comparison of the average Nusselt number.

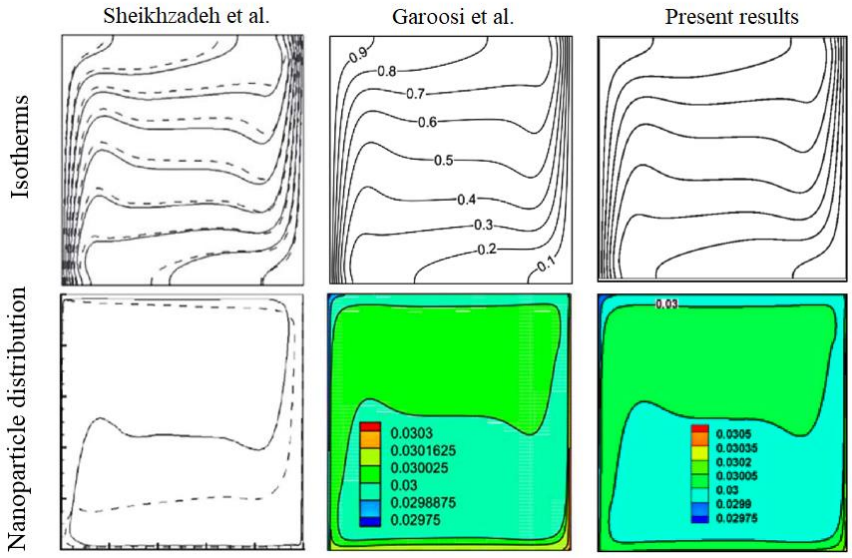

Fig. 3. Comparison of current results with those of Sheikhzadel et al. [43] Garoosi et al. [14]

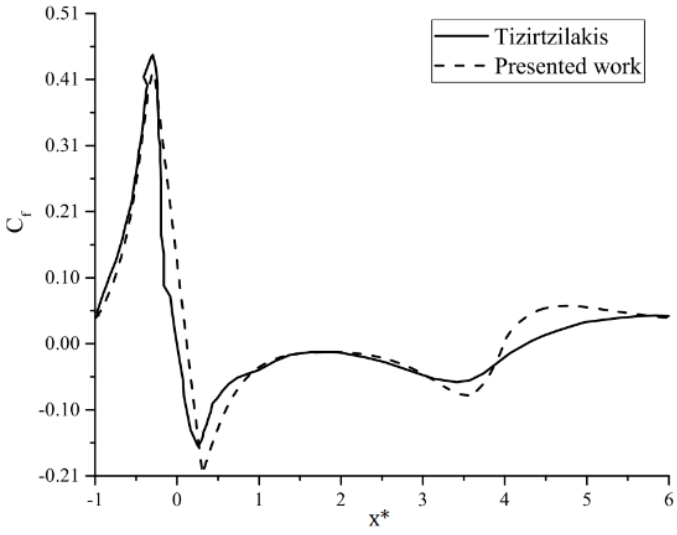

Fig. 4. Comparison of local friction coefficient

relative error between the experimental and current numerical results is determined to be 7.9% indicating the acceptable agreement. The difference between measured and predicted Nusselt numbers can be mainly attributed to different correlations used for the estimation of the thermophysical properties of nanofluids.

Another comparison is made with the results of Refs. [42] and [15]. Isotherms and the distribution of particles are shown in Fig. 3. According to the figure, the agreement is excellent. To further check the accuracy of the current results, a comparison is made by the results of Tzirtzilakis [43], who numerically investigated a biomagnetic fluid flow in an aneurysm and under a non-uniform magnetic field. The axial variation of the friction factor is depicted in Fig. 4. The results are in good agreement, with small differences due to the different numerical methods used in the two studies (finite difference vs. finite volume).

Finally, the present results are compared with those of Basak et al. [44]. They analyzed the mixed convection problem in a porous enclosure. The distribution of local Nusselt number along the left and right walls are compared in Fig. 5. Once again, the agreement is good, with an average relative error of less than 6%. This error can be related to the various techniques employed in the two studies (finite element vs. finite volume).

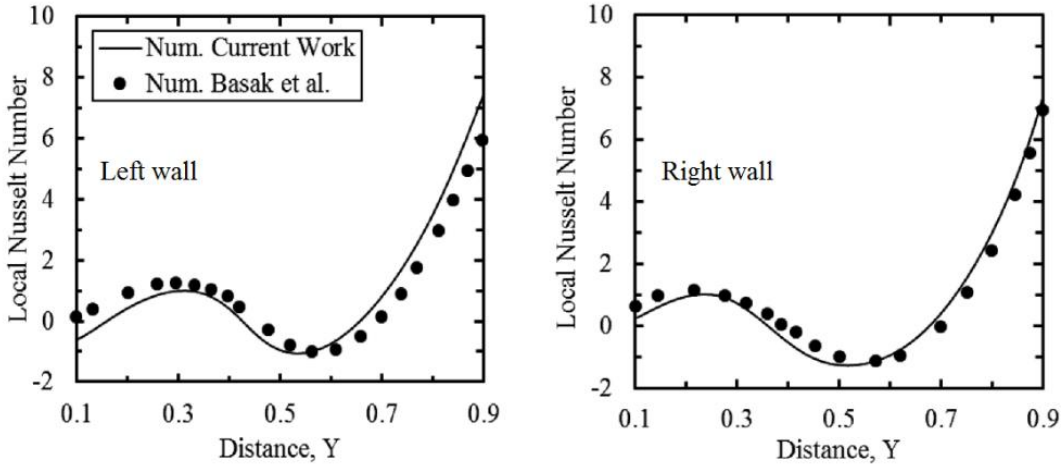

Fig. 5. Comparison of current results with those of Basak et al. [45] for Gr = 10^5, Re=10, Pr=10 and Da=10^{-3}

4- Results and Discussion

The MHD-FHD effects on the free convection of a magnetic nanofluid in a porous media are studied numerically utilizing Buongiorno's two-phase model and based on the Darcy-Brinkman formulation. In this study, the Brownian, thermophoresis, and magnetophoresis fluxes of nanoparticles in the carrier fluid are taken into account. Computations are performed for different values of dimensionless numbers including Rayleigh number ($Ra = 10^4, 10^6$), Hartmann number ($Ha = 1, 3$ and 1), magnetic number ($Mn = 1\times10^7, 2\times10^7$ and 4×10^7), and porosity ($\varepsilon = 0.5, 0.9$) The effects of the above-mentioned parameters on the streamlines, temperature field, nanoparticle distribution, and the rate of heat transfer are examined. It should be noted that the values of Prandtl number, Schmidt number, Darcy number, dimensionless temperature difference (δ), and N_{BT} are kept constant at 4.623, 3.55×10^4, 10^{-3}, 161, 0.245, respectively. Also, the average particle volume fraction is set at 0.02.

4- 1- FHD impacts

The effects of non-uniform magnetic fields (arising from eight current-carrying wires) are presented in this section. It should be mentioned that here the MHD effects are neglected (Ha=0). Fig. 6 shows the effects of the magnetic number on the flow pattern at $Ra = 10^4$ for $\varepsilon = 0.5$ and 0.9. In the absence of a magnetic field, streamlines are coaxial circles indicating a weak recirculating flow. At such a small Rayleigh number, the buoyancy forces are negligible, and therefore the dominant forces are Kelvin's body forces. As a result, in both porosity ratios, the flow pattern within the cavity is strongly influenced by the magnetic forces. It can be seen that two large vortices occupy almost the entire cavity. There are also several small vortices near the magnetic sources. It is observed that the number and size of formed vortices are more significant around the cold wall.

The effects of the magnetic number on the temperature field at $Ra = 10^4$ for $\varepsilon = 0.5$ and 0.9 are shown in Fig. 7. As can be seen, isotherms are parallel, indicating that conduction is the dominant mechanism in heat transport. However, at high magnetic numbers and especially at $\varepsilon = 0.9$, the isotherms are slightly distorted due to strong magnetic forces.

The variation of nanoparticle distribution along the hot and cold walls of the cavity for $Ra = 10^4$ and at different Mn number is depicted in Fig. 8. In the absence of a magnetic field, the nanoparticles migrate from high-temperature to low-temperature areas, which is the result of thermophoretic forces. From the figure, it is observed that along the left wall by enhancing the magnetic number, the particle void fraction increases. Also, it can be observed that nanoparticle distributions near the magnetic sources show peaks due to magnetophoretic flux.

Fig. 9 shows the streamlines at $Ra = 10^5$ for $\varepsilon = 0.5$ and 0.9. As can be seen, the flow patterns in two porosity ratios are considerably different. Regardless of the magnetic number, flow intensity is higher at $\varepsilon = 0.9$ compared to $\varepsilon = 0.5$.

Another point is that at high magnetic numbers, there are small vortices in the right-bottom corner of the enclosure due to the Kelvin body forces. It is interesting to note that at $\varepsilon = 0.9$ by applying non-uniform magnetic fields, the flow intensity decrease in the cavity. In contrast, at $\varepsilon = 0.5$, the impact of the magnetic field on the flow pattern seems to be insignificant.

To examine the FHD effects on the heat transfer rate, the variations of the average Nusselt number are plotted versus the magnetic number at two Rayleigh numbers and porosity ratios in Fig. 10. At small Rayleigh number, i.e. ($Ra = 10^4$) or small porosity ratio ($\varepsilon = 0.5$) heat transfer is primarily transmitted by conduction, and therefore, regardless of Mn values, Nusselt number approximately equals unity. But at $Ra = 10^6$ and $\varepsilon = 0.9$, the applied magnetic field declines the rate of heat transfer. These findings are consistent with the influences of magnetic field on the flow and temperature fields shown in Figs. 6, 7, and 9.

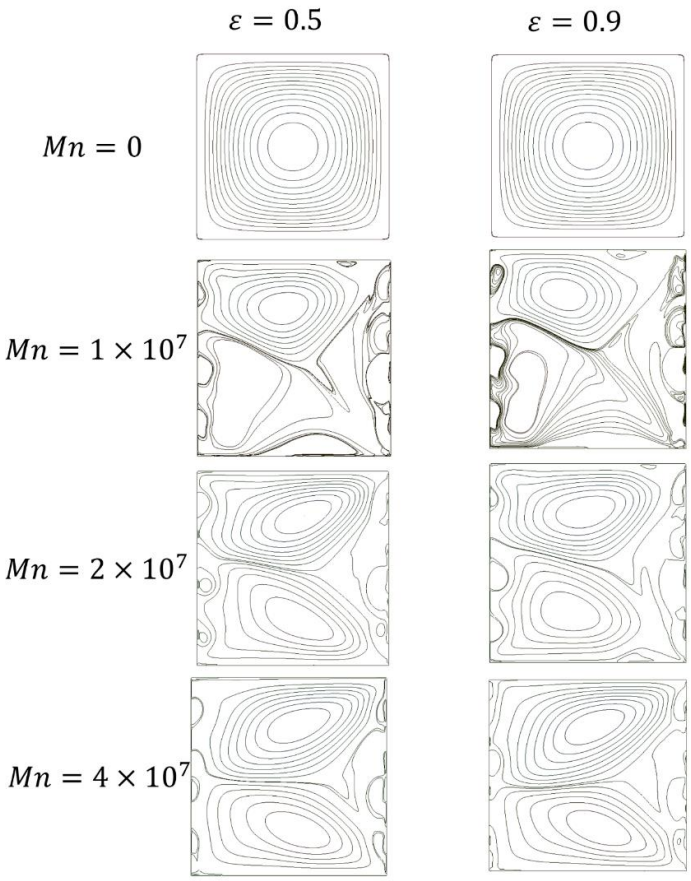

Fig. 6. Streamlines at different magnetic numbers for $Ra = 10^4$

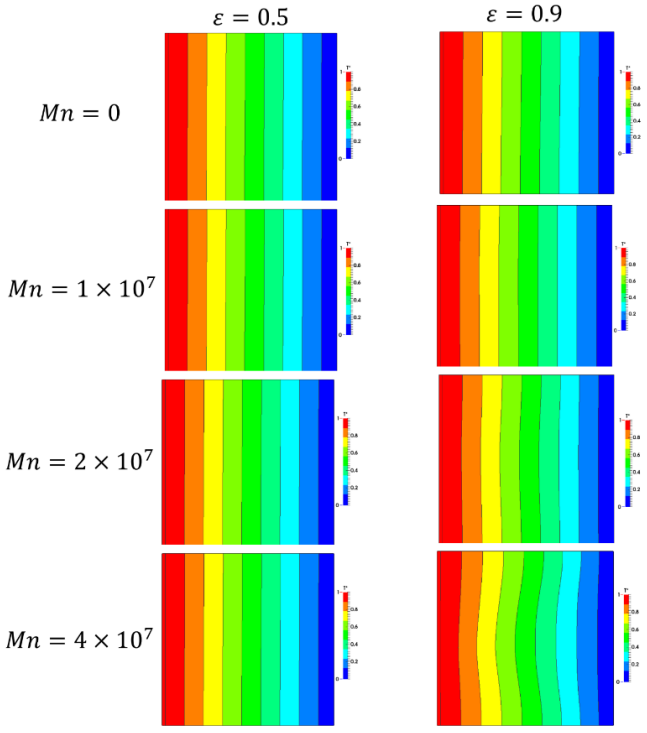

Fig. 7. Isotherms at different magnetic numbers for $Ra = 10^4$

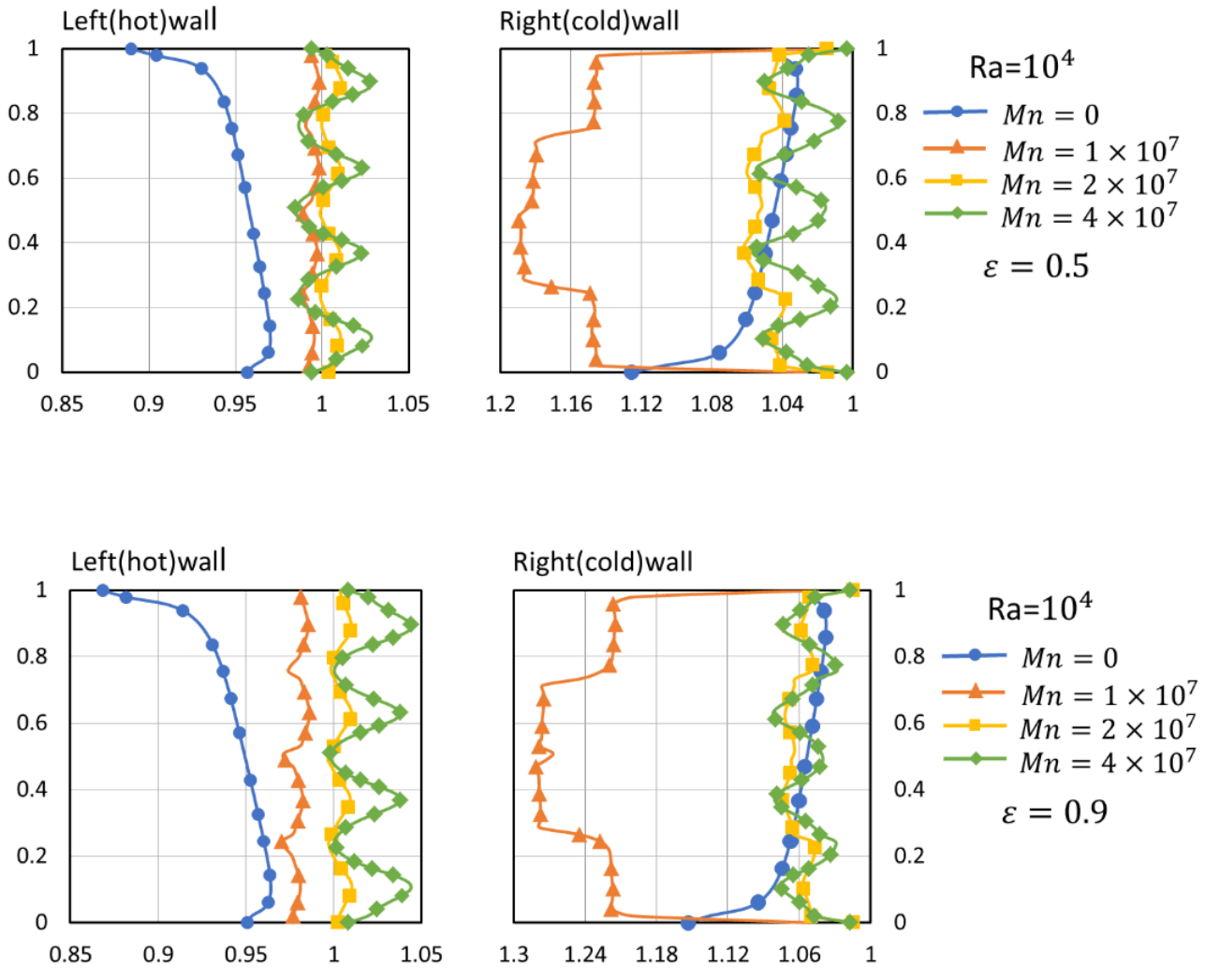

Fig. 8. nanoparticle distribution along the hot and cold walls for $Ra = 10^4$

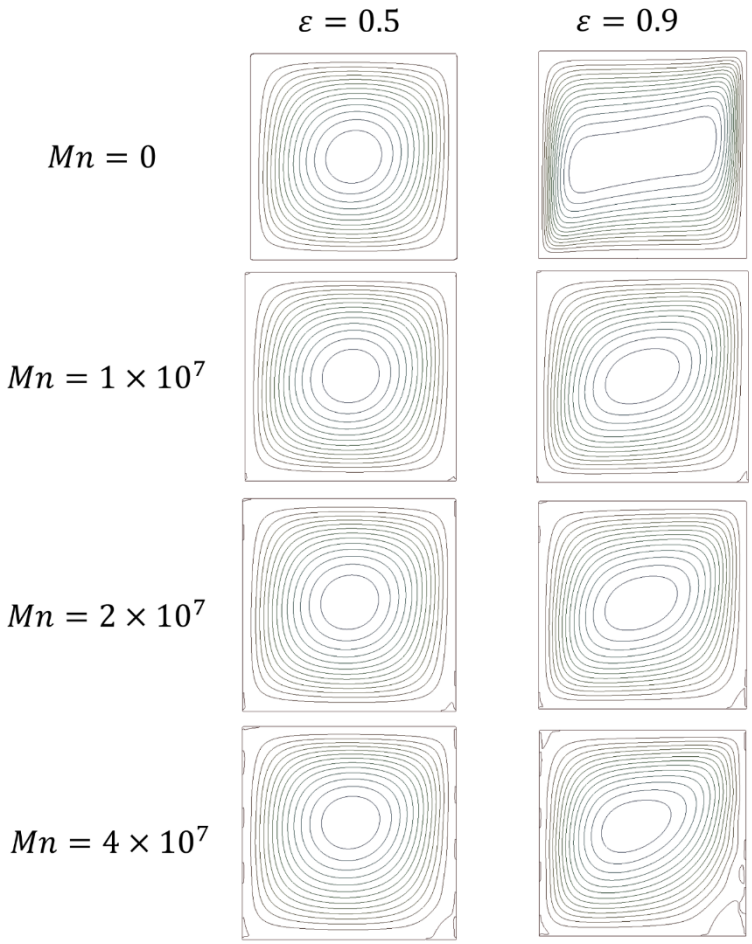

Fig. 9. Streamlines at different magnetic numbers for $Ra = 10^6$

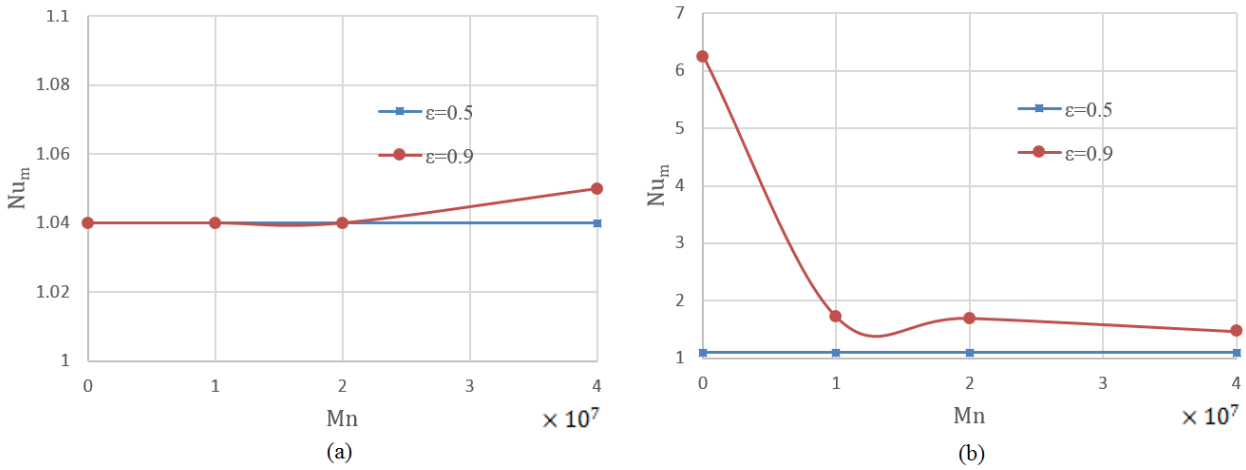

Fig. 10. The impact of the magnetic number on the rate of heat transfer: (a) $Ra = 10^4$ **(b)** $Ra = 10^6$

4- 2- MHD impacts

The impact of MHD (due to a uniform magnetic field) on the flow variables is discussed in this section. It should be noted that here the magnetic number is taken to be $Mn = 0$.

The influence of Hartmann number on the streamlines and isotherms at $Ra = 10^4$ for $\varepsilon = 0.5$ and 0.9 are shown in Figs. 11 and 12, respectively.

Due to negligible driven forces and also suppression of fluid flow by retarding effects of Lorentz forces, advection is weak. Consequently, apart from the Ha or ε values streamlines are coaxial circles. Besides, isotherms are parallel and therefore, heat is mainly transferred by conduction.

The distribution of nanoparticles along vertical walls of the cavity is plotted in Fig. 13 at various Hartmann numbers. In the absence of MHD effects (Ha=0), the distribution of nanoparticles is affected by Brownian and thermophoresis fluxes. As can be seen, the concentration of particles on the hot wall is lower, and on the cold wall is higher, and applying a uniform magnetic field has no considerable impact on the overall distribution of the nanoparticles.

Fig. 14 shows the influence of Hartmann number on the streamlines at $Ra = 10^6$ for $\varepsilon = 0.5$ and $\varepsilon = 0.9$. In both porosity ratios, it is seen that at high Hartmann numbers the flow is retarded due to the Lorentz forces.

Fig. 15 illustrates the variation of Nu as a function of Ha at two Rayleigh numbers and porosity ratios. At $Ra = 10^4$, there is weak advection therefore, irrespective of the porosity ratio, the applied uniform magnetic field has a negligible impact on the rate of heat transfer. Consequently, the mean Nusselt number is independent of the Hartmann number and is nearly 1.0. At $Ra = 10^6$ and higher porosity ratio, the applied magnetic field declines Nu value. By comparing Figs. 15 and 10, it can be seen that the MHD and FHD effects on the rate of heat transfer are similar.

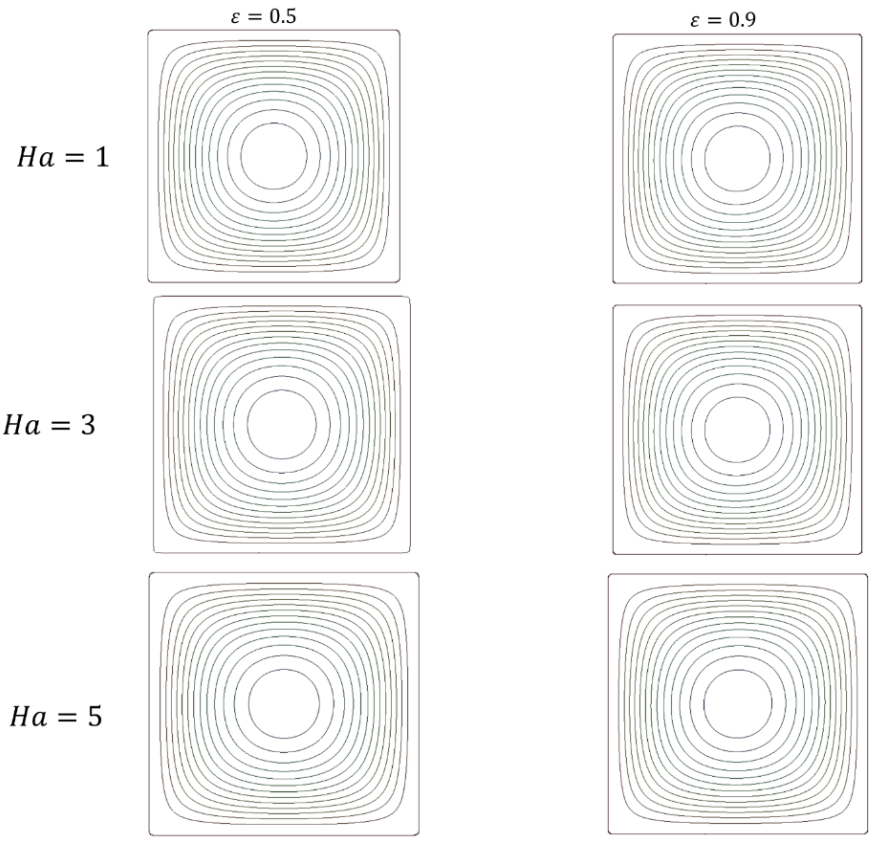

Fig. 11. Streamlines at different Hartmann numbers for $Ra = 10^4$

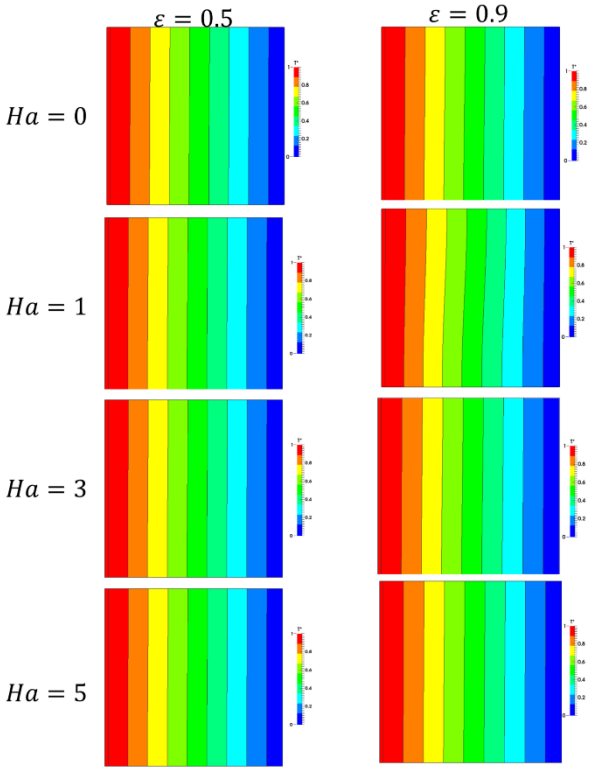

Fig. 12. Isotherms at different Hartmann numbers for $Ra = 10^4$

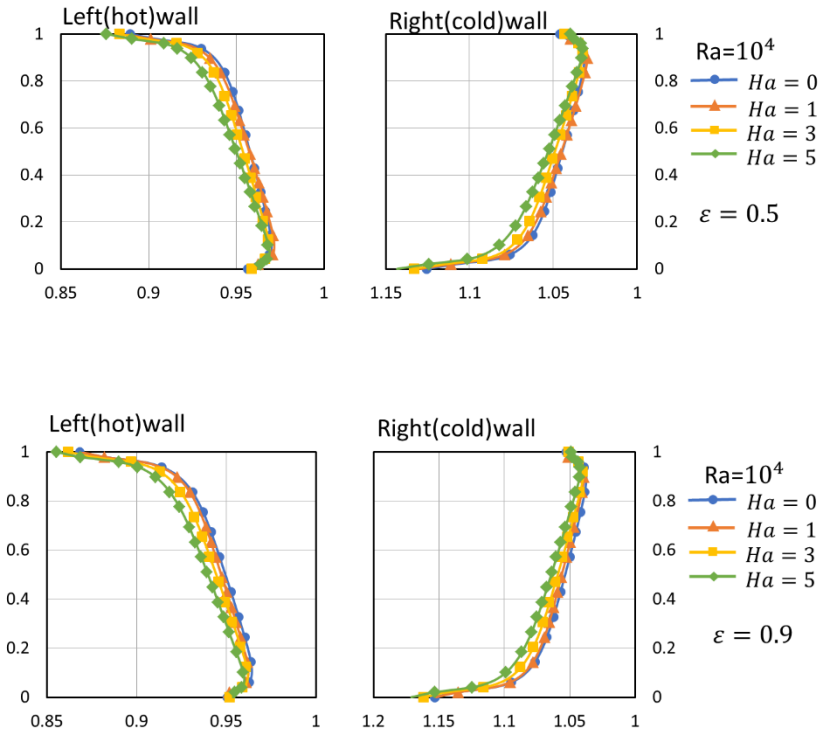

Fig. 13. nanoparticle distribution along the hot wall (left) and the cold wall (right) for $Ra = 10^4$

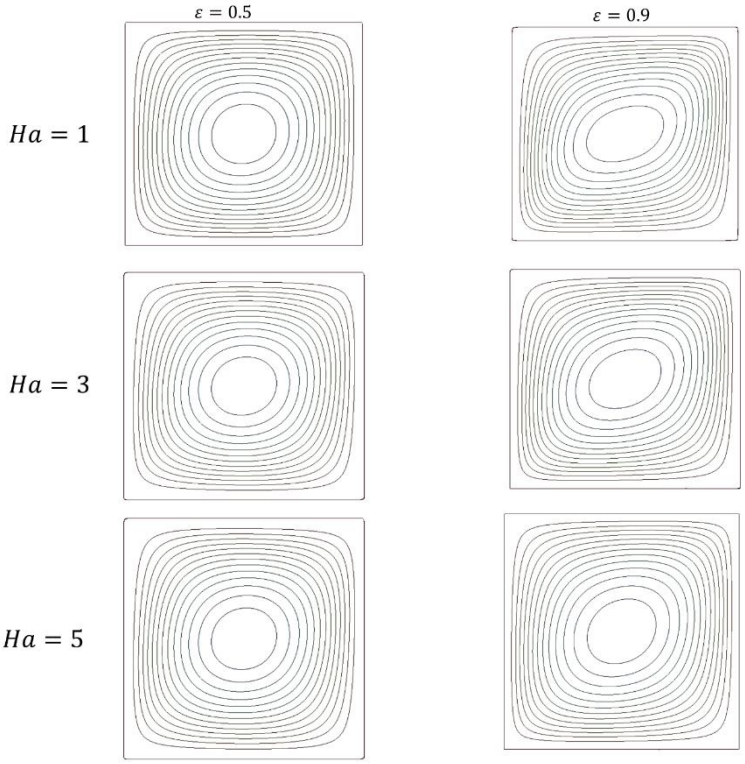

Fig. 14. streamlines at various Hartmann numbers for $Ra = 10^6$

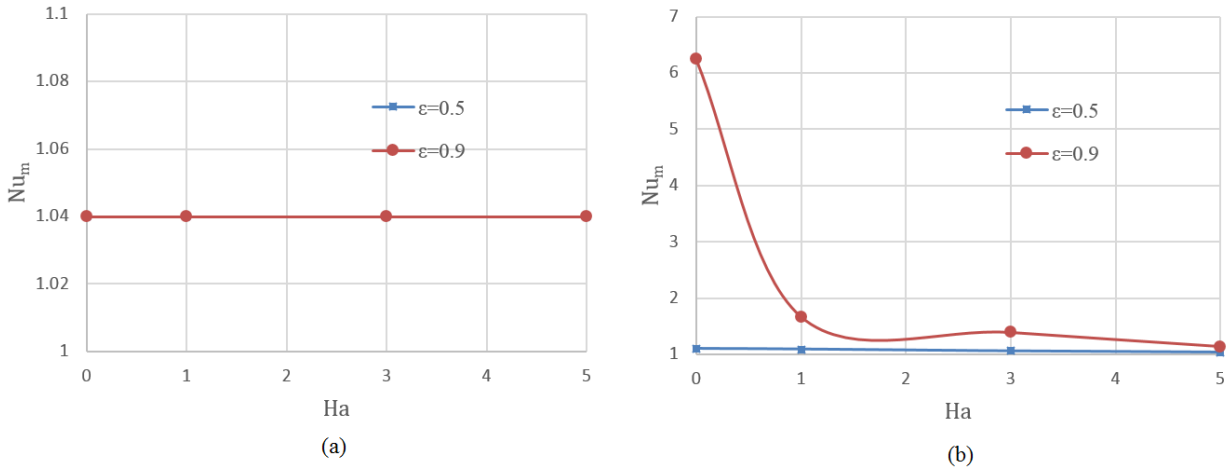

Fig. 15. Nu vs. Hartmann number: (a) $Ra = 10^4$ **(b)** $Ra = 10^6$

4- 3- Simultaneous impacts of FHD and MHD

Simultaneously impacts of FHD and MHD on the flow variables are discussed in this section. Streamlines at $Ra = 10^4$ and $\varepsilon = 0.5$ are depicted at different magnetic and Hartmann numbers in Fig. 16.

As expected, the flow pattern is more complicated because of the existence of Kelvin, Lorentz, and buoyancy forces. As can be seen, the main flow structure consists of two large counter-rotating vortices. Moreover, there are several small vortices near the magnetic sources. As shown, at high magnetic numbers the flow is thoroughly driven by the Kelvin body forces.

Fig. 17 shows the isotherms for $Ra = 10^4$ and $\varepsilon = 0.5$ at different Mn and Ha numbers. Since the flow is weak irrespective of Mn and Ha values isotherms are parallel, which indicates that heat is predominantly transmitted by the conduction.

Fig. 18. shows the particle distribution along the hot and cold walls of cavity isotherms for $Ra = 10^4$ and $\varepsilon = 0.5$ at different Mn and Ha numbers. For specified values of Ha, when the Mn increases the nanoparticle void fraction increases along the hot walls.

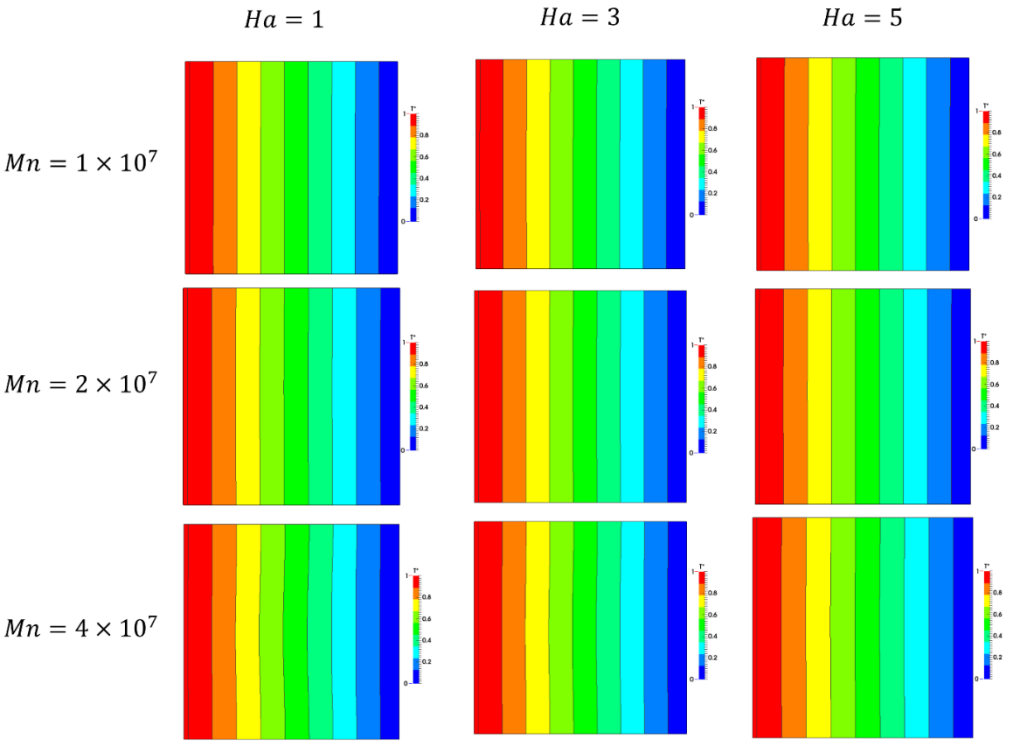

Fig. 17. Isotherms at different Ha and Mn values for $Ra = 10^4$

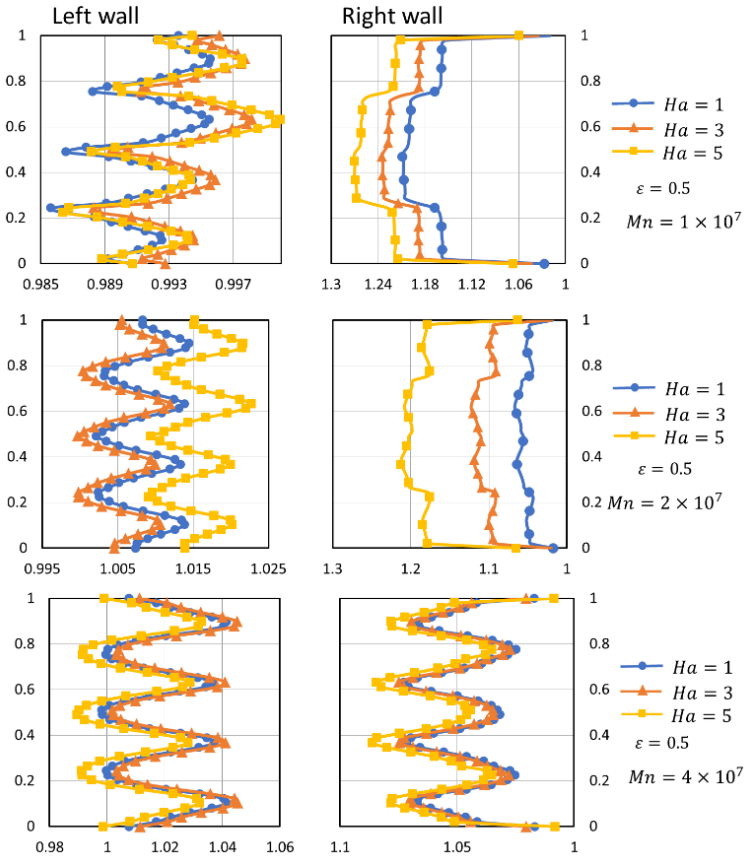

Fig. 18 Nanoparticle distribution along the vertical walls for $Ra = 10^4$ and various values of Ha and Mn

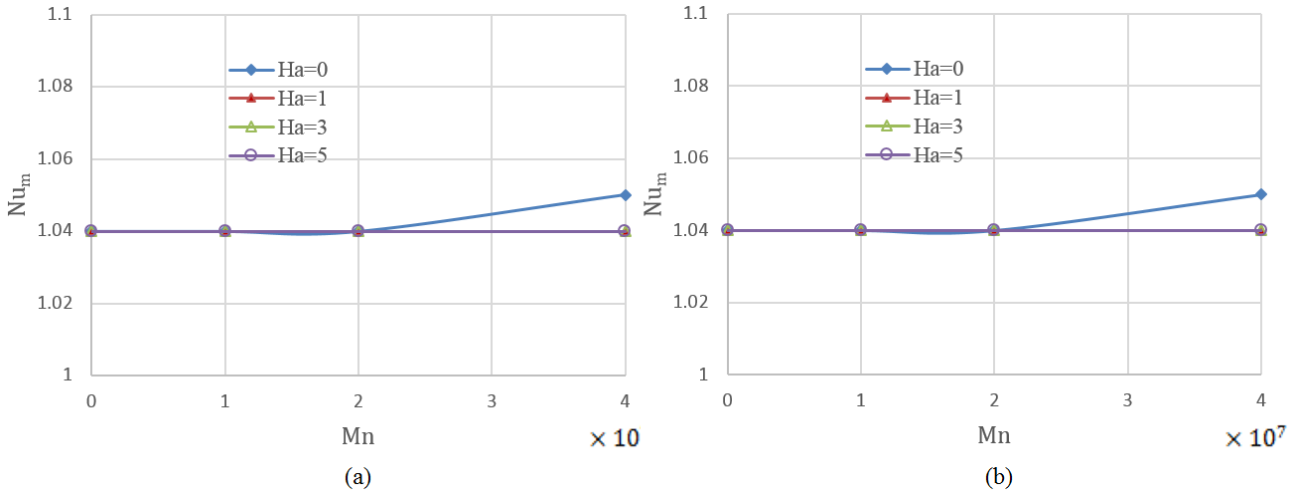

Fig. 19. Effect of Mn and Ha on the mean Nusselt number for $Ra=10^4$: (a) $\varepsilon=0.5$ (b) $\varepsilon=0.9$

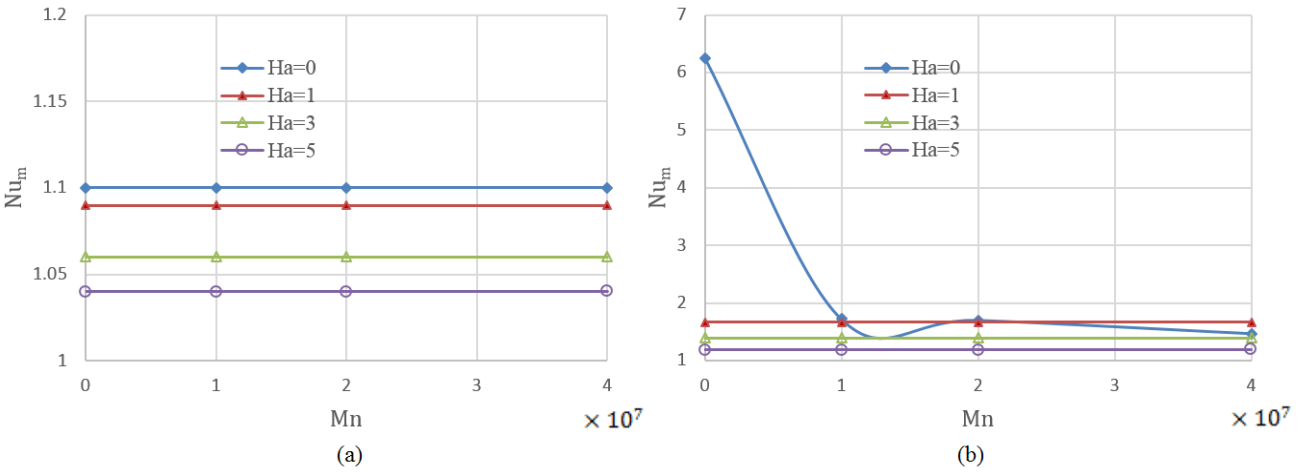

Fig. 20. Impact of Mn and Ha on the mean Nusselt number for $Ra=10^6$: (a) $\varepsilon=0.5$ (b) $\varepsilon=0.9$

The mean Nusselt number for $Ra=10^4$ and $\varepsilon=0.5$ and 0.9 is plotted at different magnetic and Hartmann numbers in Fig. 19. According to the figure and in the range of studied parameters it is concluded that at $Ra=10^4$ the heat is essentially transferred by conduction. Therefore, the average Nusselt number value is nearly independent of Ha, Mn, and ε.

Fig.20 illustrates the variation of mean Nusselt with Mn and Ha for and $Ra=10^4$ at two porosity ratios. As can be seen, in comparison with MHD the FHD effects on the heat transfer rate are almost negligible. Irrespective of the porosity ratio, the rate of heat exchange decreases with an increasing Hartmann number.

5- Conclusion

The impacts of FHD and MHD on the natural convection of a magnetic nanofluid in a porous enclosure are studied by a two-phase model and based on the finite volume method. The published literature shows that the magnetic nanofluid convection problems have been mostly simulated by the single-phase model. In the present work, a two-phase model is used to consider the effects of Brownian diffusion, thermophoresis, and magnetophoresis of particles. The influences of some critical factors such as Rayleigh, magnetic, and Hartmann numbers, and also the porosity ratio of porous media on the temperature and flow fields, nanoparticle distribution of magnetic nanoparticles, and the mean Nusselt number are

presented. It is found that due to the magnetophoresis effect, the magnetic nanoparticle void fraction increases in proximity to the magnetic sources. Also, thermophoresis effects lead to the migration of particles from the hot to the cold wall. Numerical results indicate that at $Ra=10^4$ the heat transfer rate is influenced neither by FHD nor by MHD effects. Besides, at $Ra=10^6$ FHD effects can be ignored in comparison with MHD ones. At $Ra=10^6$ and $\varepsilon=0.9$, the average Nusselt number is decreased from 6.25 to 1.4 and 1.2 due to FHD and MHD effects, respectively.

Nomenclature

D_B Brownian diffusivity, [m^2 s^{-1}]

D_T Thermophoresis diffusivity, [m^2 s^{-1}]

Da Darcy number, [-]

$\vec{\mathbf{H}}$ Intensity of magnetic field, [A m^{-1}]

Ha Hartmann number, [-]

I Electrical current, [A]

$\vec{\mathbf{J}}$ Flux vector of particles, [kg m^{-2} s^{-1}]

K Permeability, [m^2]

k Thermal conductivity, [W m^{-1} K^{-1}]

k_B Boltzmann's constant (=1.38066×10^{-23}), [J K^{-1}]

Side length of the cavity, [m]

$L(\varepsilon)$ Langevin function, [-]

Le Lewis number, [-]

$\vec{\mathbf{M}}$ Magnetization, [A m^{-1}]

Mn Magnetic number, [-]

m_p Magnetic moment, [A m^2]

N_{BT} Brownian to thermophoretic diffusions, [-]

Nu Nusselt number, [-]

P Pressure, [N m^{-2}]

Pr Prandtl number, [-]

Ra Rayleigh number, [-]

Sc Schmidt number, [-]

T Temperature, [K]

$\vec{\mathbf{V}}$ velocity field, [m s^{-1}]

Greek symbols

α Thermal diffusivity, [m^2 s^{-1}]

β Volumetric expansion coefficient, [K^{-1}]

ε Porosity, [-]

ξ Langevin parameter, [-]

μ Viscosity, [kg m^{-1} s^{-1}]

μ_0 Vacuum permeability, [T.m A^{-1}]

Bohr magneton, [A m^2]

ρ Density, [kg m^{-3}]

φ Void fraction, [-]

Subscripts

eff Effective

f Base fluid

m Mean

nf Nanofluid

p Nanoparticle

s Solid matrix

References

[1] S.U. Choi, J.A. Eastman, Enhancing thermal conductivity of fluids with nanoparticles, Argonne National Lab., IL (United States), 1995.

[2] K. Khanafer, K. Vafai, M. Lightstone, Buoyancy-driven heat transfer enhancement in a two-dimensional enclosure utilizing nanofluids, International journal of heat and mass transfer, 46(19) (2003) 3639-3653.

[3] S. Soleimani, M. Sheikholeslami, D. Ganji, M. Gorji-Bandpay, Natural convection heat transfer in a nanofluid filled semi-annulus enclosure, International Communications in Heat and Mass Transfer, 39(4) (2012) 565-574.

[4] M. Sheikholeslami, R. Ellahi, M. Hassan, S. Soleimani, A study of natural convection heat transfer in a nanofluid filled enclosure with elliptic inner cylinder, International Journal of Numerical Methods for Heat & Fluid Flow, (2014).

[5] H. Soltanipour, S. Khalilarya, S.Y. Motlagh, I. Mirzaee, The effect of position-dependent magnetic field on nanofluid forced convective heat transfer and entropy generation in a microchannel, Journal of the Brazilian Society of Mechanical Sciences and Engineering, 39(1) (2017) 345-355.

[6] M. Akbari, N. Galanis, A. Behzadmehr, Comparative analysis of single and two-phase models for CFD studies of nanofluid heat transfer, International Journal of Thermal Sciences, 50(8) (2011) 1343-1354.

[7] S. Göktepe, K. Atalık, H. Ertürk, Comparison of single and two-phase models for nanofluid convection at the entrance of a uniformly heated tube, International Journal of Thermal Sciences, 80 (2014) 83-92.

[8] A.I. Alsabery, T. Armaghani, A.J. Chamkha, M.A. Sadiq, I. Hashim, Effects of two-phase nanofluid model on convection in a double lid-driven cavity in the presence of a magnetic field, International Journal of Numerical Methods for Heat & Fluid Flow, (2019).

[9] P. Barnoon, D. Toghraie, R.B. Dehkordi, H. Abed, MHD mixed convection and entropy generation in a lid-driven cavity with rotating cylinders filled by a nanofluid using two phase mixture model, Journal of Magnetism and Magnetic Materials, 483 (2019) 224-248.

[10] D. Kashyap, A.K. Dass, Effect of boundary conditions on heat transfer and entropy generation during two-phase mixed convection hybrid Al2O3-Cu/water nanofluid flow in a cavity, International Journal of Mechanical Sciences, 157 (2019) 45-59.

[11] A. Razeghi, I. Mirzaee, M. Abbasalizadeh, H. Soltanipour, Al 2 O 3/water nano-fluid forced convective flow in a rectangular curved micro-channel: first and second law analysis, single-phase and multi-phase approach, Journal of the Brazilian Society of Mechanical Sciences and Engineering, 39(6) (2017) 2307-2318.

[12] J. Buongiorno, Convective transport in nanofluids, (2006).

[13] M. Corcione, M. Cianfrini, A. Quintino, Two-phase mixture modeling of natural convection of nanofluids with temperature-dependent properties, International Journal of Thermal Sciences, 71 (2013) 182-195.

[14] H. Azimikivi, N. Purmahmud, I. Mirzaee, Rib shape and nanoparticle diameter effects on natural convection heat transfer at low turbulence two-phase flow of AL2O3-water nanofluid inside a square cavity: Based on Buongiorno's two-phase model, Thermal Science and Engineering Progress, 20 (2020) 100587.

[15] F. Garoosi, S. Garoosi, K. Hooman, Numerical simulation of natural convection and mixed convection of the nanofluid in a square cavity using Buongiorno model, Powder technology, 268 (2014) 279-292.

[16] S.Y. Motlagh, H. Soltanipour, Natural convection of Al2O3-water nanofluid in an inclined cavity using Buongiorno's two-phase model, International Journal of Thermal Sciences, 111 (2017) 310-320.

[17] S.Y. Motlagh, M.M. Youshanloei, T. Safabakhsh, Numerical investigation of FHD pump for pumping the magnetic nanofluid inside the microchannel with hydrophobic walls, Journal of the Brazilian Society of Mechanical Sciences and Engineering, 41(5) (2019) 1-16.

[18] A. Sharifi, S.Y. Motlagh, H. Badfar, Numerical investigation of magnetic drug targeting using magnetic nanoparticles to the Aneurysmal Vessel, Journal of Magnetism and Magnetic Materials, 474 (2019) 236-245.

[19] A. Sharifi, S. Yekani Motlagh, H. Badfar, Investigation of the effects of two parallel wires' non-uniform magnetic field on heat and biomagnetic fluid flow in an aneurysm, International Journal of Computational Fluid Dynamics, 32(4-5) (2018) 248-259.

[20] H. Soltanipour, A. Gharegöz, M.B. Oskooee, Numerical study of magnetic field effect on the ferrofluid forced convection and entropy generation in a curved pipe, Journal of the Brazilian Society of Mechanical Sciences and Engineering, 42(3) (2020) 1-15.

[21] G.R. Kefayati, Effect of a magnetic field on natural convection in an open cavity subjugated to water/alumina nanofluid using Lattice Boltzmann method, International Communications in Heat and Mass Transfer, 40 (2013) 67-77.

[22] M. Sheikholeslami, M. Gorji-Bandpy, Free convection of ferrofluid in a cavity heated from below in the presence of an external magnetic field, Powder technology, 256 (2014) 490-498.

[23] E. Tzirtzilakis, M. Xenos, Biomagnetic fluid flow in a driven cavity, Meccanica, 48(1) (2013) 187-200.

[24] A. Kasaeian, R. Daneshazarian, O. Mahian, L. Kolsi, A.J. Chamkha, S. Wongwises, I. Pop, Nanofluid flow and heat transfer in porous media: a review of the latest developments, International Journal of Heat and Mass Transfer, 107 (2017) 778-791.

[25] M.A. Sheremet, T. Groşan, I. Pop, Free convection in shallow and slender porous cavities filled by a nanofluid using Buongiorno's model, Journal of heat transfer, 136(8) (2014) 082501.

[26] M.A. Sheremet, I. Pop, M.M. Rahman, Three-dimensional natural convection in a porous enclosure filled with a nanofluid using Buongiorno's mathematical model, International Journal of Heat and Mass Transfer, 82 (2015) 396-405.

[27] S.Y. Motlagh, S. Taghizadeh, H. Soltanipour, Natural convection heat transfer in an inclined square enclosure filled with a porous medium saturated by nanofluid using Buongiorno's mathematical model, Advanced Powder Technology, 27(6) (2016) 2526-2540.

[28] S.Y. Motlagh, E. Golab, A.N. Sadr, Two-phase modeling of the free convection of nanofluid inside the inclined porous semi-annulus enclosure, International Journal of Mechanical Sciences, 164 (2019) 105183.

[29] D. Nield, A. Bejan, Convection in porous media, Fifth, in, Springer-Verlag, New York, 2016.

[30] H. Aminfar, M. Mohammadpourfard, S.A. Zonouzi, Numerical study of the ferrofluid flow and heat transfer through a rectangular duct in the presence of a non-uniform transverse magnetic field, Journal of Magnetism and Magnetic materials, 327 (2013) 31-42.

[31] M.I. Shliomis, B.L. Smorodin, Convective instability of magnetized ferrofluids, Journal of Magnetism and Magnetic Materials, 252 (2002) 197-202.

[32] Y. Pak BCCho, Hydrodynamic and heat transfer study of dispersed fluids with submicron metallic oxide particles, Exp Heat Trans, 11 (1998) 151170.

[33] Y. Xuan, W. Roetzel, Conceptions for heat transfer correlation of nanofluids, International Journal of heat and Mass transfer, 43(19) (2000) 3701-3707.

[34] H.C. Brinkman, The viscosity of concentrated suspensions and solutions, The Journal of chemical physics, 20(4) (1952) 571-571.

[35] R. Hamilton, Crosser, 0. K.," Thermal Conductivity of Heterogeneous Two-Component Systems," Industrial and Engineering Chemistry, Fundamentals, 1 (1962) 187-191.

[36] J.C. Maxwell, A treatise on electricity and magnetism, Clarendon press, 1873.

[37] Q. Xiong, M. Izadi, E. Assareh, Natural heat exchange in inhomogeneous porous medium using linear and quadratic porosity distribution, International Journal of Thermal Sciences, 161 (2021) 106731.

[38] H. Aminfar, M. Mohammadpourfard, Y.N. Kahnamouei, A 3D numerical simulation of mixed convection of a magnetic nanofluid in the presence of non-uniform magnetic field in a vertical tube using two phase mixture model, Journal of Magnetism and Magnetic Materials, 323(15) (2011) 1963-1972.

[39] H. Soltanipour, Two-phase simulation of magnetic field effect on the ferrofluid forced convection in a pipe considering Brownian diffusion, thermophoresis, and magnetophoresis, The European Physical Journal Plus, 135(9) (2020) 1-23.

[40] S.V. Patankar, Numerical heat transfer and fluid flow, CRC press, 2018.

[41] C. Ho, W. Liu, Y. Chang, C. Lin, Natural convection heat transfer of alumina-water nanofluid in vertical square enclosures: An experimental study, International Journal of Thermal Sciences, 49(8) (2010) 1345-1353.

[42] G.A. Sheikhzadeh, M. Dastmalchi, H. Khorasanizadeh, Effects of nanoparticles transport mechanisms on Al2O3–water nanofluid natural convection in a square enclosure, International Journal of Thermal Sciences, 66 (2013) 51-62.

[43] E. Tzirtzilakis, Biomagnetic fluid flow in an aneurysm using ferrohydrodynamics principles, Physics of Fluids, 27(6) (2015) 061902.

[44] T. Basak, S. Roy, S.K. Singh, I. Pop, Analysis of mixed convection in a lid-driven porous square cavity with linearly heated side wall (s), International journal of heat and mass transfer, 53(9-10) (2010) 1819-1840.

HOW TO CITE THIS ARTICLE

S. Goudarzi , S. Yekani Motlagh, H. Soltanipour, Two-Phase Simulation of Magnetohydrodynamics and Ferrohydrodynamics Impacts on the Natural Convection of a Magnetic Nanofluid within a Porous Cavity, AUT J. Mech Eng., 6 (1) (2022) 129-148.

DOI: 10.22060/ajme.2021.19819.5967